IOP Publishing Journal of Physics D: Applied Physics

J. Phys. D: Appl. Phys. **51** (2018) 165101 (7pp) https://doi.org/10.1088/1361-6463/aab5a7

Deviatoric stresses promoted metallization in rhenium disulfide

Yukai Zhuang[1,2], Lidong Dai[1], Heping Li[1], Haiying Hu[1], Kaixiang Liu[1,2], Linfei Yang[1,2], Chang Pu[1,2], Meiling Hong[1,2] and Pengfei Liu[3]

[1] Key Laboratory of High-Temperature and High-Pressure Study of the Earth's Interior, Institute of Geochemistry, Chinese Academy of Sciences, Guiyang, Guizhou 550081, People's Republic of China
[2] University of Chinese Academy of Sciences, Beijing 100049, People's Republic of China
[3] State Key Laboratory of Structural Chemistry, Fujian Institute of Research on the Structure of Matter, Chinese Academy of Sciences, Fuzhou, Fujian 350002, People's Republic of China

E-mail: dailidong@vip.gyig.ac.cn

Received 6 December 2017, revised 13 February 2018
Accepted for publication 9 March 2018
Published 28 March 2018

Abstract

The structural, vibrational and electronic properties of ReS_2 were investigated up to ~34 GPa by Raman spectroscopy, AC impedance spectroscopy, atomic force microscopy and high-resolution transmission electron microscopy, combining with first-principle calculations under two different pressure environments. The experimental results showed that ReS_2 endured a structural transition at ~2.5 GPa both under non-hydrostatic and hydrostatic conditions. We found that a metallization occurred at ~27.5 GPa under non-hydrostatic conditions and at ~35.4 GPa under hydrostatic conditions. The occurrence of distinct metallization point attributed to the influence of deviatoric stresses, which significantly affected the layered structure and the weak van der Waals interaction for ReS_2.

Keywords: high pressure, deviatoric stress, layered materials, diamond-anvil cell, metallization

S Supplementary material for this article is available online

(Some figures may appear in colour only in the online journal)

Introduction

Strain has a significant influence on the electronic, transport, and optical properties of semiconductors [1, 2], especially for the two-dimensional (2D) crystals as it can sustain much larger strains than bulk crystals in the structures [3]. For example, previous studies reported that graphene can be strained up to the yield strength without any structural distortion [4]. This provides a very useful approach to tune on the mechanical and electronic properties of 2D materials. Among the 2D family, the anisotropic 2D materials [5, 6] have one more degree of freedom to deliver various physical properties than isotropic materials like graphene and MoS_2 [7]. For instance, the absence of intrinsic energy band-gap obstructs the further application of graphene in logic and memory devices, which require high on–off ratio and low off-state current [8]. And the MoS_2 monolayer has a low carrier mobility, which limits its application in high-performance future field-effect transistors (FETs) [9, 10].

Two dimensional (2D) layered transition metal dichalcogenides (LTMD) have attracted great interest, due to their novel physical properties and excellent device prospects [11, 12]. Rhenium disulphide (ReS_2), a new member of LTMD family, is a promising material suitable for TMD-based optoelectronic nano-devices with robust sizable and direct band-gap semiconducting characteristics [13], where one monolayer consists of one lattice of rhenium atoms which is sandwiched between two lattices of sulphur atoms. However, the ReS_2 does not crystallize in a 2H structure but in a distorted CdCl structure due to charge decoupling from an additional valence electron in the rhenium atoms, which leads to a reduced crystal symmetry [14]. The distorted structure and the low crystal symmetry are connected with the Peierls mechanism [14, 15], which prevents ordered stacking and minimizes the

interlayer overlap of wave functions. Thus, unlike some other semiconducting LTMDs which will change from indirect to direct band-gap when going from the bulk to monolayer [16, 17], the bulk properties of ReS_2 are close to those of single layer and the interlayer interaction is rather weak [14].

Since the optical and electronic properties of ReS_2 can be not modified so much with increasing layers, stress and pressure become a more effective way to change the properties of ReS_2 as they can directly modify the lattice parameters, symmetrize the structure and remove the Peierls distortion [18]. Meanwhile, some novel physical properties displayed by LTMDs under pressure can also be significant issues, such as phase transition and metallization. For LTMDs, interlayer interaction, driven by weak van der Waals (vdW) interactions, plays an important role in varying physical properties of LTMDs [7]. And it is remarkable sensitive to the deviatoric stress. For instance, MoS_2 can be induced an irreversible metallization under deviatoric stress [19]. Therefore, artificially made deviatoric stress rather than hydrostatic pressure may significantly affect the electronic properties of 2D materials [20, 21], especially for the anisotropic 2D LTMDs. In light of this, we systematically explored the properties of anisotropic multilayer ReS_2 in high-pressure both at non-hydrostatic and hydrostatic conditions.

In this work, using efficient crystal and electronic structure research methods including impedance spectroscopy, Raman spectroscopy, atomic force microscopy (AFM), high-resolution transmission electron microscopy (HRTEM) and temperature-dependent conductivity measurements in conjunction with first-principle calculations, we reported a structural phase transition and metallization of ReS_2 under both non-hydrostatic and hydrostatic conditions up to ~34 GPa. In addition, the metallization of ReS_2 delayed nearly 8 GPa under hydrostatic conditions than that of under non-hydrostatic conditions. Our results revealed that deviatoric stress played a significant role in modifying the electronic structure in the anisotropic 2D LTMDs, which confirmed our theoretical calculations well in predicting the metallization.

Experimental methods

The ReS_2 powder sample was purchased from Alfa-Aesar (99.999%). All observed data of the AFM and TEM images were collected via a Multimode 8 mass spectrometer (Bruker) and Tecnai G2 F20 S-TWIN TMP, respectively. The high-pressure Raman experiments were conducted in a 300 μm anvil culet diamond anvil cell (DAC). Similar to the previous work, the pressure was calibrated with the wavenumber shift of the fluorescence bands in the Cr^{3+} of ruby sphere [22]. The pressure medium for hydrostatic conditions was the 4:1 mixture of methanol and ethanol. A Renishaw 2000 Raman Spectrometer (TCS SP8, Leica) was used to collect the Raman spectra with an Olympus CCD camera. Spectra were taken by using an argon ion laser (Spectra Physics; 514.5 nm, power <1 mW) with a spectral resolution of 1.0 cm^{-1} in the range of 300–550 cm^{-1} in the quasi-backscattering geometry. Each collected spectra was sustained for 450 s. And the DAC pressure standstill time was 900 s before spectral acquisition in order to achieve the stable equilibrium. Raman spectra were fitted using the PeakFit software. A linear baseline calibration was applied and a Lorenztian curve was assumed during the fitting.

High-pressure electrical studies were carried out by a DAC with a 300 μm anvil culet. A T-301 gasket was pre-indented for a 40 μm thickness, and a 180 μm center hole was drilled by a laser. Then it was filled by the mixed powder of boron nitride and epoxy, and another 100 μm center hole was drilled as the insulating sample chamber. A Solartron-1260 AC impedance spectroscopy analyzer was used to implement the electrical conductivity measurements at frequencies of 10^{-1}–10^{7} Hz. The specific measurement procedures were described in detail [23, 24]. And the deformation of the diamond anvils during measurement process was also taken into account [25]. First-principles calculations were performed using density functional theory and the pseudo potential methods [26] on the standard CASTEP code in the Material Studio package. The exchange and correlation terms were described in the generalized gradient approximation (GGA) with the Perdew–Burke–Ernzerhof (PBE) scheme. Structural optimizations were carried out using the Broyden–Fletcher–Goldfarb–Shanno (BFGS) minimization algorithm [27]. A kinetic cut off energy of 450 eV, and appropriate Monkhorst–Pack k-point meshes ($6 \times 6 \times 3$ meshes) were set up for all structures to ensure the convergence of the enthalpy calculations.

Results and discussion

High-pressure Raman spectra were performed to study the structural properties of ReS_2 both at non-hydrostatic and hydrostatic conditions (figure 1 and supplementary figure 1 (stacks.iop.org/JPhysD/51/165101/mmedia)). In the present work, most of the expected Raman-active modes could be seen [28], and three prominent Raman peaks (150, 161 and 212 cm^{-1}) corresponding to the in-plane vibration modes (E_{g1}, E_{g2} and E_{g3}) were selected to further analyse [29].

As can be seen from figure 1(b), the Raman shift decreased with pressure before ~2.5 GPa and then gradually increased after ~2.5 GPa under non-hydrostatic conditions. The drastic change at this pressure point may be owed to a phase transition from the distorted-3R to distorted-1T [18], which induced with a relative sliding between sandwiched layers. And there was a similar trend existed in that of hydrostatic conditions (supplementary figure 1). It may because that the deviatoric stresses can be ignored if pressure is not high enough (figure 1(a) inset). In fact, a previous study has reported that the non-hydrostatic deviatoric stresses were very small below 2.14 GPa [30]. Besides, the phase transition was reversible as the Raman spectra recovered after decompression both under non-hydrostatic and hydrostatic conditions.

Figure 2 exhibited the representative Nyquist plots from impedance spectroscopy at different pressures to understand the electrical properties of ReS_2. Firstly, both the semi-circular arcs, representing the grain boundary and grain interior resistance, gradually increased with pressure, then after ~3 GPa the

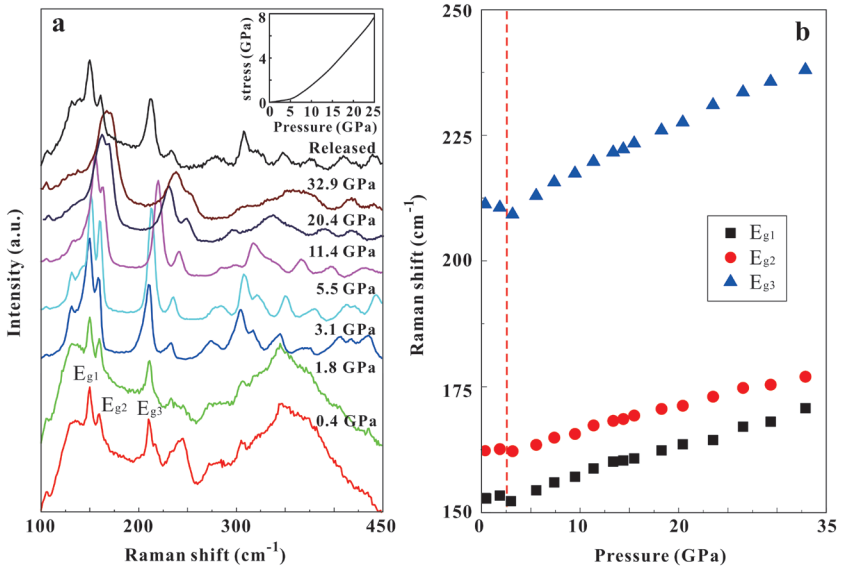

Figure 1. Raman spectroscopic results of ReS_2 under non-hydrostatic condition. (a) Raman spectra at representative pressure points. Inset: the positive relevance between pressure and the deviatoric stress. (b) The Raman shifts of the selected modes with increasing pressure.

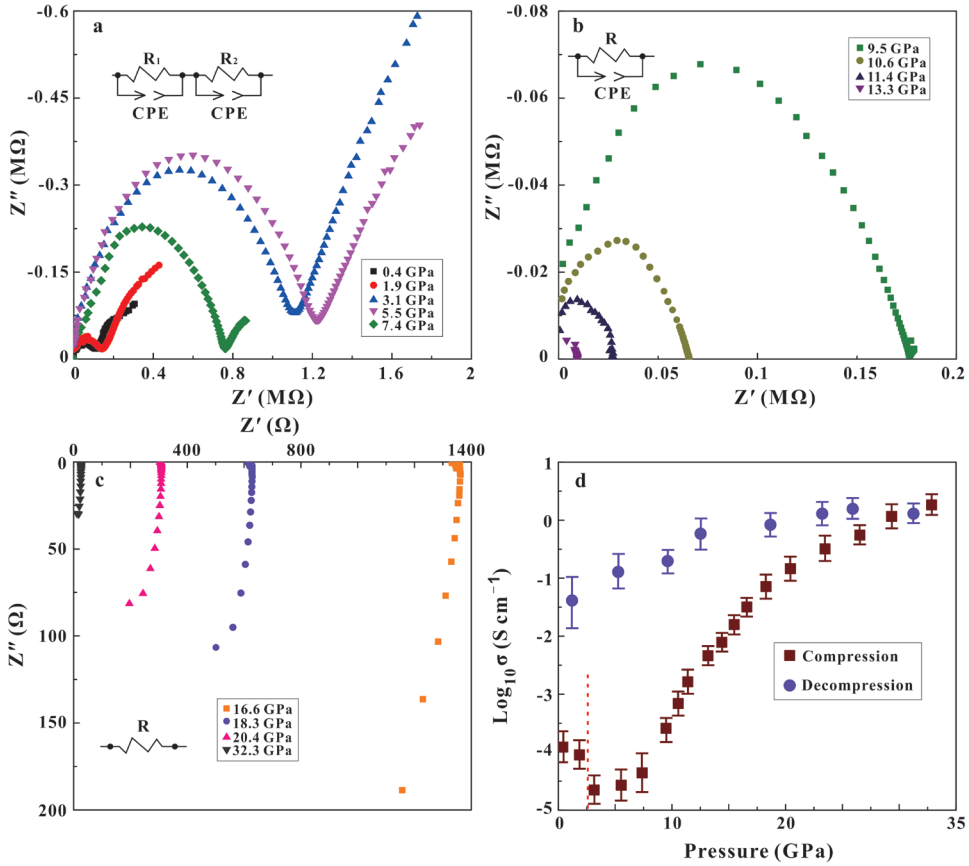

Figure 2. The electronic properties of ReS_2 under non-hydrostatic conditions. (a)–(c) Nyquist plots from the impedance spectra at different pressures. (b) Pressure-dependent electrical conductivity of ReS_2.

semi-circular arcs decreased and the grain boundary resistance disappeared at approximately ~9.5 GPa. Next, the impedance spectra only displayed in the fourth quadrant after ~15 GPa (figure 2(c)), which indicates that the electronic crystal structure of ReS_2 greatly changed, and it may demonstrate a pressure-induced electronic polarization [31].

From figure 2(d), the electrical conductivity of ReS_2 decreased to a pressure of ~2.5 GPa and suddenly increased after that under non-hydrostatic conditions. We attributed the abrupt change point to a phase transition, which was consistent with the Raman data. Moreover, the conductivity tended to be stable when pressure up to ~27.5 GPa. And the conductivity

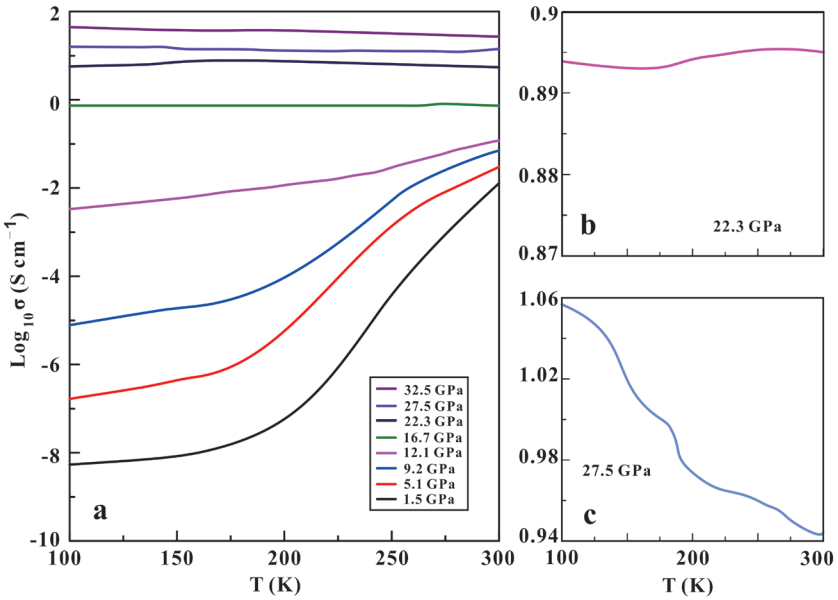

Figure 3. (a) The pressure dependence of conductivity of ReS_2 as a function of temperature under non-hydrostatic conditions. (b) The temperature-dependent conductivity of ReS_2 at ~22.3 GPa. (c) The temperature-dependent conductivity of ReS_2 at ~27.5 GPa.

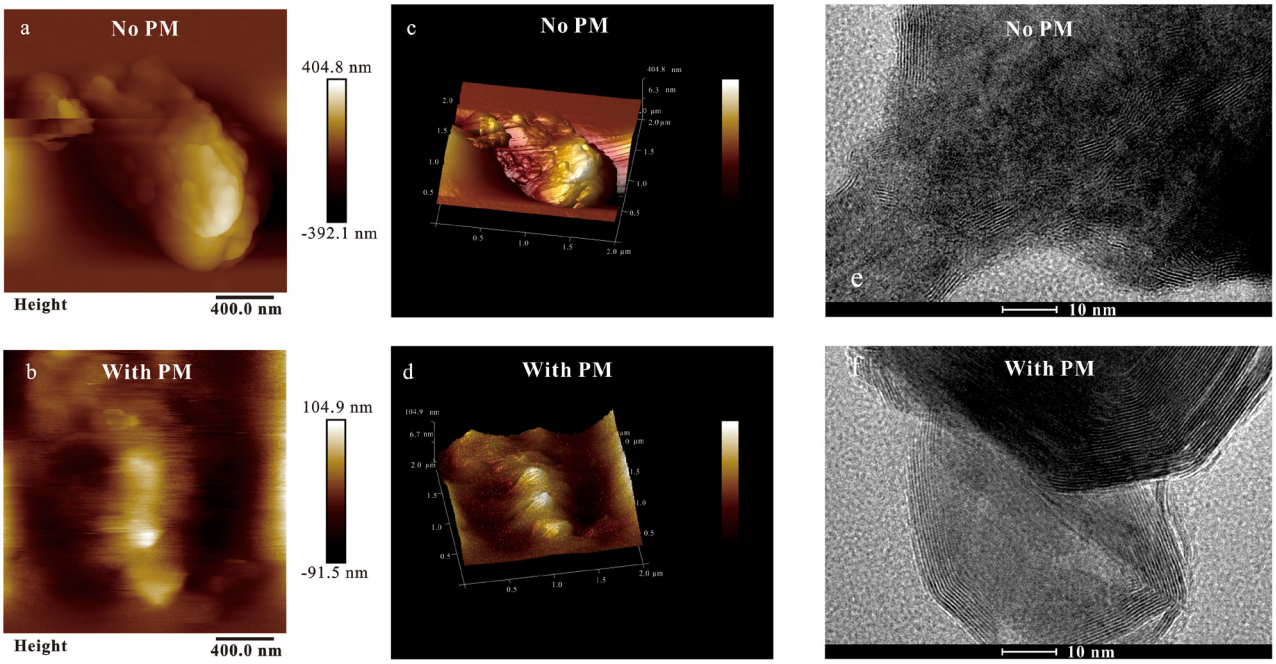

Figure 4. (a) AFM image of the pressure-induced morphology of decompressed ReS_2 from 33.1 GPa under non-hydrostatic conditions, (c) related 3D AFM picture. (b) AFM image of decompressed ReS_2 from 34.2 GPa under hydrostatic conditions, (d) related 3D AFM picture. (e) and (f) HRTEM images of decompressed ReS_2 from 33.3 GPa under non-hydrostatic conditions and 34.1 GPa under hydrostatic conditions, respectively. PM: pressure medium.

value indicated that the ReS_2 may be metallized after this pressure point. Furthermore, to mutually verify these results, the temperature-dependent conductivity measurements of ReS_2 were executed.

As shown in figure 3(a), the conductivity of ReS_2 increased with an increasing temperature before 12.1 GPa, which was a typical semiconductor characterization. Then the conductivity sloped gently between 12.1 GPa and 27.5 GPa (figure 3(b)), which was the intermediate state between semiconductor and metal. In fact, the intermediate state from semiconductor to metal also existed in other material [32]. Since 27.5 GPa, the conductivity decreased with an increasing temperature and an available variation of 12% electrical conductivity was observable at the temperature from 100 K to 300 K, displaying a typical metal behaviour (figure 3(c)). As the main conduction mechanism in metal is free electrons. With temperature up, the scattering effect on free electrons is enhanced by thermal vibration of crystal lattice, which reduces the conductivity [33]. Besides, the similar variation trend also appeared in other layer structural material [27]. Therefore, the results

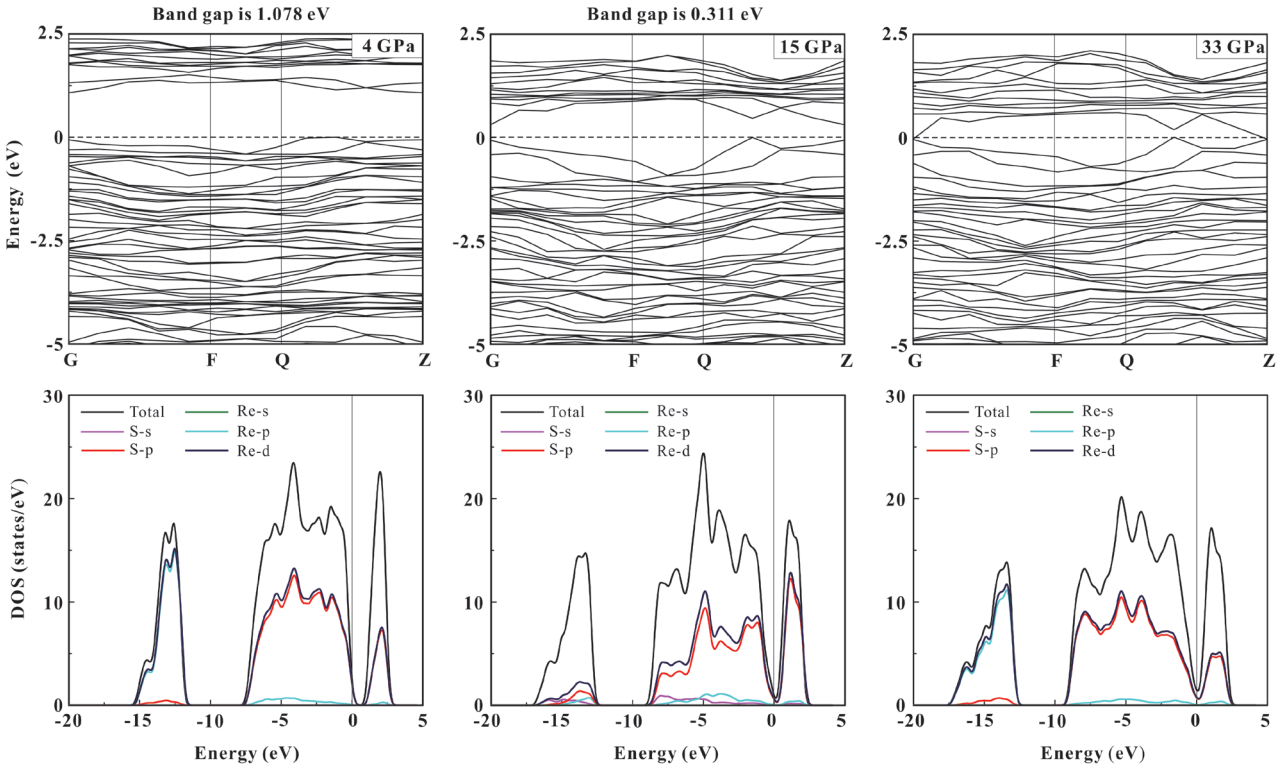

Figure 5. The calculated band structure and corresponding total and partial density of ReS_2 at selected pressures under non-hydrostatic conditions. (a) 4 GPa, (b) 15 GPa and (c) 33 GPa. The semiconductor of ReS_2 changes to metal with increasing pressure.

of the temperature-dependent conductivity measurements clearly certified the metallization of ReS_2 at a high pressure. For hydrostatic conditions, the pressure point of metallization was 35.4 GPa (supplementary figure 2). The distinct delay of metallization under hydrostatic conditions may due to the influence of deviatoric stresses. Actually, it is well recognized that deviatoric stresses play a significant effect on compression measurements [34]. Some experiments even showed that the metallization of other material was dependent on the degree of deviatoric stresses [35]. For non-hydrostatic conditions, the distortion of the geometry of the unit cells and the molecules under deviatoric stresses leads to the lowering of symmetry, and a stronger interaction will be generated in the interlayer of ReS_2 and results in the observed metallization changes [36, 37].

To reveal the morphology and structural change of ReS_2 after metallization for further study, AFM and HRTEM were applied to the decompressed samples (figure 4). Figure 4(a) showed the surface morphology of ReS_2 after decompression under non-hydrostatic conditions. The results demonstrated that it was destroyed and difficult to distinguish the surface layers. However, from figure 4(b), the surface-layered morphology was well preserved and could be clearly discerned after decompression under hydrostatic conditions. Meanwhile, for HRTEM, after decompression under non-hydrostatic conditions, the layered structure of ReS_2 was drastically disordered. However, from figure 4(d), the layered structure preserved perfectly under hydrostatic conditions after decompression. These displayed results clearly exhibited the role that deviatoric stresses played in this electronic structure transition. A previous study has indicated that the degree of deviatoric stresses could affect the metastability of the quenched materials, and it was the deviatoric stresses rather than absolute pressure that acted as a more important role in phase transition [38]. For non-hydrostatic conditions, the ReS_2 may be suffered from much stronger stress due to the existing of deviatoric stress, and stronger interlayer interactions may produce more intense attraction to change structure and are more likely to yield a continuous lattice response [39], which may promote the occurrence of metallization.

Figure 5 and supplementary figure 3 showed the theoretical calculation results under non-hydrostatic and hydrostatic conditions, respectively. And the required stresses, in non-hydrostatic conditions, are based on the experimental data (as shown in the inset of figure 1(a), for example, the deviatoric stress reached ~8 GPa, while the center pressure was ~25 GPa). The calculated band structure results obviously revealed that ReS_2 has a theoretical direct band-gap of 1.371 eV at room pressure (supplementary figure 3), which was well consistent with a previous study [14]. It is worth noting that compared to Heyd–Scuseria–Ernzerhof (HSE) hybrid functional and the Green's function and screened Coulomb interaction (GW) methods, although PBE usually underestimates the band-gap of 2D materials, the decreased trend of band-gap under high-pressure is correct [20], which related to the metallization. The band-gap gradually decreased with increasing pressure and reached 0 at 33 GPa under non-hydrostatic conditions, which indicated a semiconductor-to-metal transition. This theoretical result was coincident with our experimental data, confirming the metallization of ReS_2 near ~27.5 GPa. Also,

from the projected density of states (DOS) of figure 5, one can see that the highest occupied valence bands and the conduction bands, located around the Fermi energy, were essentially dominated by the Re-d state and additional contributions from the S-p state, which hybridized with each other [40]. And the extent of hybridization and electronic coupling increased with pressure, which results in the diffusion of the valence bands and conduction bands. Besides, with the increasing pressure, the high-energy valence bands widen stronger than that of the conduction bands, leading to the decrease of band-gap and the increase of electrical conductivity for ReS_2. Additionally, the pressure point of theoretical metallization was ~9 GPa higher under hydrostatic conditions than that of under non-hydrostatic conditions. Previous studies have indicated that it was the overlap of the conduction band and valence band that induced the metallization [41, 42]. For LTMDs, the shrink of interlayer spacing between layers under high pressure will lead to the decrease of the band-gap. Then the conduction band and valence band overlap when the band-gap becomes zero, which finally results in the metallization [19]. Meanwhile, for ReS_2, the layered anisotropic material, the band-gap could decrease with the increasing compressive or tensile uniaxial strain and it also decreases with the increasing shear strain [43]. It means that, compared to the isotropic LTMDs [19], ReS_2 is more sensitive to the deviatoric stress due to the anisotropic structure, which leads to the ahead of ~9 GPa in the pressure point of metallization under non-hydrostatic conditions. Thus, our obtained first-principle theoretical calculations results pay more attention on the significant effect of the deviatoric stress, which is in good consistency with the experimental observations from the measurements of Raman scattering and electrical conductivity at high pressure.

Conclusions

The high pressure behaviours of ReS_2 were investigated systematically including the structural, vibrational and electronic properties by using a series of experimental methods, containing the impedance spectroscopy, temperature-dependent conductivity measurements, Raman spectroscopy, AFM and HRTEM, in conjunction with the theoretical calculations. In the present work, ReS_2 underwent a phase transition from distorted-3R to distorted-1T phase at nearly ~2.5 GPa both under non-hydrostatic and hydrostatic conditions. Furthermore, a transformation from a semiconductor to metal occurred at ~27.5 GPa under non-hydrostatic conditions and ~35.4 GPa under hydrostatic conditions, respectively. In this process, we emphasize the significant influence of deviatoric stresses in promoting the occurrence of metallization. These high-pressure properties displayed by ReS_2 will help us further understand the universal crystal structure evolution and electrical property patterns of LTMDs.

Acknowledgments

This research was financially supported by the Strategic Priority Research Program (B) of the Chinese Academy of Sciences (XDB 18010401), Key Research Program of Frontier Sciences of CAS (QYZDB-SSW-DQC009), '135' Program of the Institute of Geochemistry of CAS, Hundred Talents Program of CAS and NSF of China (41474078, 41774099 and 41772042). The support of the Supercomputer Center of Fujian Institute of Research on the Structure of Matter (FJIRSM) is acknowledged.

ORCID iDs

Lidong Dai https://orcid.org/0000-0002-9081-765X

References

[1] Haeni J H *et al* 2004 *Nature* **430** 758
[2] Lai K, Nakamura M, Kundhikanjana W, Kawasaki M, Tokura Y, Kelly M A and Shen Z X 2010 *Science* **329** 190
[3] Yu S, Zhu H, Eshun K, Arab A, Badwan A and Li Q 2015 *J. Appl. Phys.* **118** 164306
[4] Gómez-Navarro C, Burghard M and Kern K 2008 *Nano Lett.* **8** 2045
[5] Liu E *et al* 2015 *Nat. Commun.* **6** 6991
[6] Zhao H, Wu J, Zhong H, Guo Q, Wang X, Xia F, Yang L, Tan P and Wang H 2015 *Nano Res.* **8** 3651
[7] Mak K F, Lee C, Hone J, Shan J and Heinz T F 2010 *Phys. Rev. Lett.* **105** 136805
[8] Britnell L *et al* 2012 *Science* **335** 947
[9] Fuhrer M S and Hone J 2013 *Nat. Nanotechnol.* **8** 146
[10] Zhang S, Zhou W, Ma Y, Ji J, Cai B, Yang S A, Zhu Z, Chen Z and Zeng H 2017 *Nano. Lett.* **17** 3434
[11] Benavente E, Santa Ana M A, Mendizábal F and González G 2002 *Coordin. Chem. Rev.* **224** 87
[12] Zeng H, Dai J, Yao W, Xiao D and Cui X 2012 *Nat. Nanotechnol.* **7** 490
[13] Yu Z G, Cai Y and Zhang Y W 2015 *Sci. Rep.* **5** 13783
[14] Tongay S *et al* 2014 *Nat. Commun.* **5** 3252
[15] Kertesz M and Hoffmann R 1984 *J. Am. Chem. Soc.* **106** 3453
[16] Ponomarenko L A *et al* 2011 *Nat. Phys.* **7** 958
[17] Radisavljevic B, Radenovic A, Brivio J, Giacometti V and Kis A 2011 *Nat. Nanotechnol.* **6** 147
[18] Zhou D *et al* 2017 *NPJ Quantum Mater.* **2** 19
[19] Zhuang Y, Dai L, Wu L, Li H, Hu H, Liu K, Yang L and Pu C 2017 *Appl. Phys. Lett.* **110** 122103
[20] Zhang S *et al* 2018 *Chem. Soc. Rev.* **47** 982
[21] Zhang S, Yan Z, Li Y, Chen Z and Zeng H 2015 *Angew. Chem. Int. Ed.* **54** 3112
[22] Jayaraman A 1983 *Rev. Mod. Phys.* **55** 65
[23] Hu H, Dai L, Li H, Hui K and Li J 2015 *Solid State Ion.* **276** 136
[24] Dai L, Hu H, Li H, Wu L, Hui K, Jiang J and Sun W 2016 *Geochem. Geophys. Geosyt.* **17** 2394
[25] Dai L, Zhuang Y, Li H, Wu L, Hu H, Liu K, Yang L and Pu C 2017 *J. Mater. Chem.* C **5** 12157
[26] Segall M D, Lindan P J D, Probert M J, Pickard C J, Hasnip P J, Clark S J and Payne M C 2002 *J. Phys.: Condens. Matter* **14** 2717
[27] Dai L, Liu K, Li H, Wu L, Hu H, Zhuang Y, Yang L, Pu C and Liu P 2018 *Phys. Rev.* B **97** 024103
[28] Wolverson D and Hart L S 2016 *Nanoscale Res. Lett.* **11** 250
[29] Cui Y, Lu F and Liu X 2017 *Sci. Rep.* **7** 40080
[30] Zhao J and Ross N L 2015 *J. Phys.: Condens. Matter* **27** 185402
[31] Kandrina Y A, Babushkin A N, Shkerin S N and Volkova Y 2002 *Defect Diffus. Forum* **208–9** 295
[32] Dias R P, Kim M and Yoo C-S 2016 *Phys. Rev.* B **93** 104107

[33] Ashcroft N W and Mermin N D 1976 *Solid State Physics* (New York: Harcourt College Publishers) p 1
[34] Meng Y, Weidner D J and Fei Y 1993 *Geophys. Res. Lett.* **20** 1147
[35] Clarke D R, Kroll M C, Kirchner P D, Cook R F and Hockey B J 1988 *Phys. Rev. Lett.* **60** 2156
[36] Asahara Y, Hirose K, Ohishi Y, Hirao N, Ozawa H and Murakami M 2013 *Am. Mineral.* **98** 2053
[37] Yang F, Lin Y, Dahl J E, Carlson R M and Mao W L 2014 *J. Chem. Phys.* **141** 154305
[38] Lin Y, Yang Y, Ma H, Cui Y and Mao W L 2011 *J. Phys. Chem.* C **115** 9844
[39] Zhao Z *et al* 2015 *Nat. Commun.* **6** 7312
[40] Liu H, Xu B, Liu J M, Yin J, Miao F, Duan C G and Wan X G 2016 *Phys. Chem. Chem. Phys.* **18** 14222
[41] Zhang X, Qiao X F, Shi W, Wu J B, Jiang D S and Tan P H 2015 *Chem. Soc. Rev.* **44** 2757
[42] Ju W, Li T, Wang H, Yong Y and Sun J 2015 *Chem. Phys. Lett.* **622** 109
[43] Li Y-L, Li Y and Tang C 2017 *Int. J. Hydrog. Energy* **42** 161